ELSEVIER

Magnetic Resonance Imaging 22 (2004) 467–473

MAGNETIC RESONANCE IMAGING

A modified logistic model to describe gadolinium kinetics in breast tumors

Peter J. Moate[a,*], Lawrence Dougherty[b], Mitchell D. Schnall[b], Richard J. Landis[c], Raymond C. Boston[a]

[a]*School of Veterinary Medicine, University of Pennsylvania, Kennett Square, PA, USA*
[b]*Hospital of the University of Pennsylvania, Philadelphia, PA, USA*
[c]*School of Epidemiology, University of Pennsylvania, Philadelphia, PA, USA*

Received 30 October 2003; accepted 28 January 2004

Abstract

A five-parameter modified logistic equation is presented that describes the signal enhancement in magnetic resonance dynamic contrast enhanced imaging (MRI-DCE). In this heuristic model, P_1 approximates the baseline signal, P_2 is related to the magnitude of the peak signal enhancement, P_3 is the approximate time of the maximum rate of increase of signal, P_4 is related to the maximum rate of signal enhancement, and P_5 is the terminal slope of the signal enhancement curve. Six breast tumors were studied that exhibited diverse patterns of signal enhancement, and in each case, estimated model parameters were well identified. Three of the model parameters, P_2, P_4 and P_5 describe attributes of the signal enhancement curve that have previously been shown to have diagnostic value with respect to breast cancer. Procedures for using the primary model parameters to derive a number of secondary parameters that may also have diagnostic value are discussed. Sensitivity analysis shows that the signal enhancement curve is highly sensitive to P_3 in the region of the signal intensity curve associated with rapid uptake of the contrast reagent. Consequently, frequent signal sampling in this time domain is indicated to enable identification of P_3 and sensitive fitting of the signal intensity curve. The advantages of this heuristic model compared to commonly used compartmental modeling approaches are discussed.

Keywords: MRI; Gadolinium; Signal enhancement; Model; Breast lesions

1. Introduction

In the last decade there has been increasing use of MRI contrast reagents (CR) such as gadolinium-diethylene-triamine penta-acetic acid (Gd-DTPA) for the dynamic imaging of a variety of tumors [1–6]. In tandem with the technological advances that have enabled the acquisition of large quantities of dynamic MRI data, researchers have developed a plethora of techniques to analyze such data. Analytical approaches have been classified by Tofts as being either compartmental models or heuristic models [7]. According to Tofts, all compartment models employ a compartment to represent the blood plasma, a compartment to represent the (abnormal) extravascular extracellular space (EES), and rate constants that describe known physiological processes. Tofts asserts that all compartment models measure combinations of three parameters: (1) k^{PSp} the influx volume transfer constant (min^{-1}), sometimes designated the permeability surface area product per unit volume of tissue, between plasma and EES; (2) v_e the volume of EES per unit volume of tissue ($0 < v_e < 1$); and (3) k_{ep}, the efflux rate constant (min^{-1}), which is the ratio of the first two parameters ($k_{ep} = k^{PSp}/v_e$). A number of variations on this basic theme including a Flow-limited (High Permeability) model, a Permeability-Limited Model, a Mixed Flow and Permeability-Limited Model, a Clearance Model, and a Generalized Kinetic Model have been described [8]. Many assumptions are built into these compartmental models, including the main assumption that the parameters derived from the models do indeed describe the nominated physiological processes [7,9,10]. However, in some tumors there is an initial rapid uptake of contrast reagent, followed by a less steep but prolonged uptake of the contrast reagent. Simple compartmental models can describe this type of tumor by employing a negative value for k_{ep}. However, it is not

* Corresponding author. Tel.: +610-444-6146; fax: +610-925-8123.
E-mail address: moate@vet.upenn.edu (P.J. Moate).

0730-725X/04/$ – see front matter
doi:10.1016/j.mri.2004.01.025

physiologically possible for intercompartmental rate constants to have negative values [9,11]. To overcome these types of difficulties, other researchers have developed models in which the tumor is described by up to three compartments, and the investigator must select from five different compartmental models/topologies the model that will best describe the tumor under investigation [12]. Clearly, such an experimental/arbitrary approach does not facilitate automatic classification of tumors as benign or malignant. Furthermore, compartmental analysis generally ignores delay and dispersion effects and imposes a set of unsubstantiated assumptions that may obscure interpretation [8,13].

In contrast to the compartmental model approach, heuristic models make no assumptions or inferences about the underlying physiology of a tumor, but simply attempt to describe the important features or attributes of the uptake of CR by the tumor. Such heuristic parameters include: (1) baseline signal intensity, (2) rate of enhancement, (3) time to peak enhancement, (4) peak enhancement, and (5) terminal slope. Heuristic models focus on parameters 2–5 because these have been implicated in aiding the diagnosis of malignant tumors [14].

Heuristic models vary greatly in their level of sophistication and mathematical form. Some researchers [2,15–17], have carried out simple 'manual' arithmetic manipulations of the raw data and defined signal indices such as "baseline signal intensity" as "the average of 4 pre-contrast data points" and "% enhancement ($E\%$) after 60 as:

$$E\% = \frac{S60 - S0}{S0} * 100 \tag{1}$$

where $S0$ and $S60$ are, respectively, the signal intensities at baseline and at 60 s after administration of contrast agent. Other researchers have used a variety of mathematical equations, including gamma functions, to describe the signal intensity curves [18,19].

Regardless of the type of analysis of signal intensity curves, the ultimate aim is generally to use the information embedded in these curves to improve the differential diagnosis of malignant and benign tumors. Manual data analysis may introduce unintended user bias. Gamma functions may not have the flexibility to describe all observed signal enhancement patterns.

The standard logistic function [Eq. (2)] has many of the features of a signal intensity curve since it describes a sigmoid curve with a horizontal plateau:

$$SI(t) = \frac{P_2}{\{1 + exp(-P_4 \cdot (t - P_3))\}} + P_1 \tag{2}$$

where $SI(t)$ is the signal intensity at time t, P_1 approximates the baseline signal intensity, P_2 is the amplitude of the plateau above the baseline, P_3 (s) is the time at which the maximum slope occurs and P_4 (s^{-1}) is the maximum slope. Although Eq. (2) could perhaps describe the signal enhancement of some specific benign tumors, it could not describe the typical wash-out pattern of malignant tumors where the terminal slope is quite negative, nor could it describe some types of benign tumors where the terminal slope is persistently positive. However, modification of the standard logistic equation by the inclusion of additional structure ($P_5 \cdot t$) provides the flexibility to describe signal intensity curves with either increasing or decreasing terminal slope [Eq. (3)]:

$$SI(t) = \frac{P_2 + (P_5 \cdot t)}{\{1 + exp(-P_4 \cdot (t - P_3))\}} + P_1 \tag{3}$$

where P_1, is as defined as for Eq. (2) and P_5 (s^{-1}) is the terminal slope. In this case, as can be deduced from Eq. (3) and Fig. 1, P_2 is equivalent to the signal intensity obtained at the intersection of the zero time signal axis and a tangent drawn from the terminal portion of the signal intensity curve, minus the baseline signal intensity. From Fig. 1 it can also be seen that the time P_3 now only corresponds to the time of maximum slope if P_5 is equal to zero. However, if P_5 is greater or less than zero, P_3 and P_4 will now only approximate to the time of maximum slope and the maximum slope, respectively.

This contribution describes how the modified logistic function described in Eq. (3) above can be used to accurately describe and quantify a diverse range of patterns of Gadolinium dynamic-enhancement signal intensity curves.

2. Methods

2.1. Instrumentation and imaging protocol

Approval from our Institutional Review Board was obtained prior to the start of this study. Dynamic MRI was performed on six subjects whose breast lesions or tumors had, by microscopic examination, been diagnosed as carcinoma, fibroadenoma or benign proliferative changes. MR imaging was performed on a 1.5-T Signa scanner (General Electric Medical Systems, Milwaukee, WI, USA). After informed consent, patients were placed in the scanner in the prone position, with the breast to be imaged gently compressed within a four-coil array. The contrast-enhanced images were acquired using a fast 3D spoiled gradient-recalled (TR/TE, 9/4; flip angle = 45°; ± 64 kHz sampling bandwidth, 24 cm field-of-view, 3-mm slice thickness) back-projection sequence using 512 data samples/projection with 384 projections, and 26 slices [20]. The projection angles were interleaved so that an image volume was reconstructed with a temporal resolution of ~15 s. A baseline volume was acquired followed by dynamic imaging started simultaneously with the intravenous injection of 20 mL of gadopentetate dimeglumine (Magnevist, Berlex Laboratories, Wayne, NJ, USA). Contrast was administered over a 10-s interval and followed by a saline flush. Data were acquired over the following 5-min period.

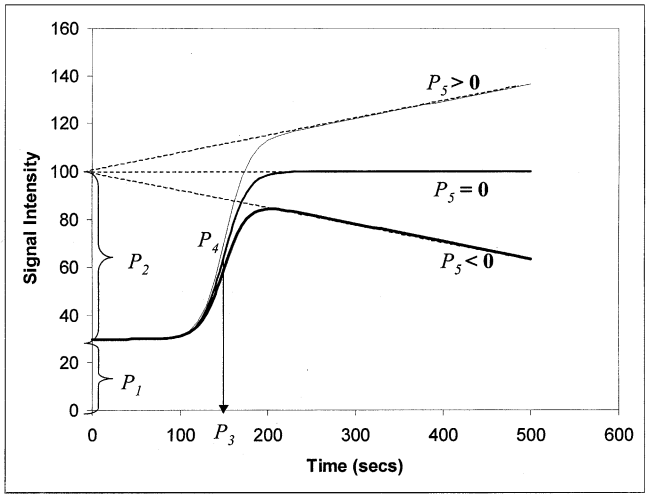

(a)

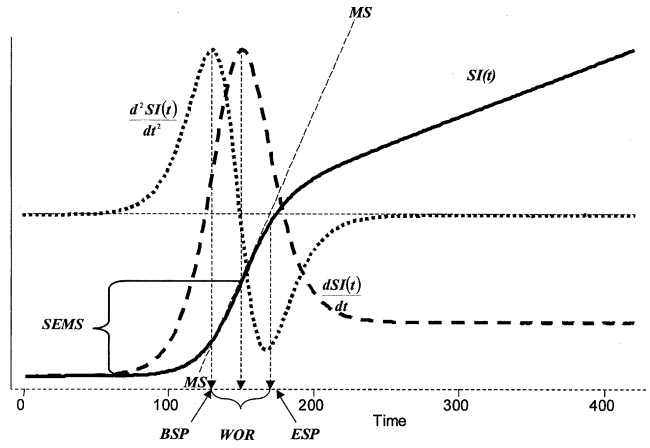

(b)

Fig. 1. (a) A schematic showing the derivation of the parameters of the modified logistic model from the dynamic signal intensity curve *SI(t)* obtained during a magnetic resonance examination of a breast tumor. P_1 represents the baseline signal, P_5 is the terminal slope (sec^{-1}), P_2 is equivalent to the a signal intensity obtained at the intersection of the zero time signal axis and a tangent drawn from the terminal portion of the signal intensity curve, minus P_1; P_3 (sec) is the time of the maximum slope and P_4 (sec^{-1}) is the maximum slope. (b) A schematic showing derivation of maximum slope (*MS*), signal enhancement at maximum slope (*SEMS*), beginning of second phase (*BSP*), end of second phase (*ESP*) and width of response (*WOR*). *SI(t)* is the Signal Intensity at time (*t*), while *dSI(t)/dt* and d^2SI/dt^2 are the first and second derivatives. Note, *SI(t)* and its first and second derivative depicted below have been rescaled to enable concurrent display. MS is depicted by the line MS-----MS.

2.2. Analysis of MR imaging data

The MRI data from each region of interest in each tumor in each patient were analyzed as follows. P_1 was calculated as the mean signal intensity of the first eight data. The remaining parameters in the modified logistic model were estimated by means of non-linear regression using STATA [21] and WinSAAM (which can be downloaded from http://www.WinSAAM.com) [22]. A number of additional parameters were derived from the parameters of the modified logistic equation. Since the signal intensity at maximum slope (*SIMS*) can be approximated by:

$$SIMS = \frac{(P_2 + P_3 * P_5)}{2} \tag{4}$$

and the signal enhancement at maximum slope (*SEMS*) was calculated by *SIMS* minus P_1.

The maximum slope (*MS*) (sec^{-1}) itself was estimated by:

$$MS = \frac{P_2 * P_4}{4} \tag{5}$$

The time of the beginning of the second phase (*BSP*) (sec) and the time of the end of the second phase (*ESP*) (sec) of the response signal were identified by determining when the maximum and minimum values occurred for the second derivative of the modified logistic equation $\left(\frac{d^2SI}{dt^2}\right)$ (see Fig. 1b). The second phase of the MRI signal curve is essentially a period when the MRI signal intensity increases in an approximately linear fashion. The width of the response (*WOR*) (sec) was calculated as the difference between *ESP* and *BSP*. The primary signal response (*PSR*) was calculated as the signal intensity at *ESP* minus P_1. The areas under the curve (in seconds), above the baseline signal intensity, between time zero and time 420 s (AUC_{420}) and also between *BSP* and *ESP* (AUC_{BE}) were determined using WinSAAM. WinSAAM was also used to carry out sensitivity analyses to determine the relative dependency of *SI(t)* on each of the principal model parameters [23]. All other post imaging calculations were made using STATA.

3. Results and Discussion

Dynamic signal intensity data and the 'best fit' time versus signal intensity curves as predicted by the modified logistic equation, for a variety of signal patterns are shown in Fig. 2. The primary and secondary parameters of the modified logistic model along with their fractional standard deviations for these same six lesions are shown in Table 1 The versatility/flexibility of the modified logistic model is shown by the fact that it was able to well describe the variety of signal patterns shown in Fig. 2 with all adjusted R^2 values greater than 0.99. With the exception of parameter P_4 for the curve shown in Fig. 2d, all parameters were well identified. Although the curve shown in Fig. 2d has an atypical shape, the modified logistic equation was still well able to describe this curve. Even for the curve shown in Fig. 2e, where data were particularly noisy, the model was able to identify the parameters of the model. The robustness of the model is further exemplified by the curve shown in Fig. 2f, where all model parameters were identified, even pa-

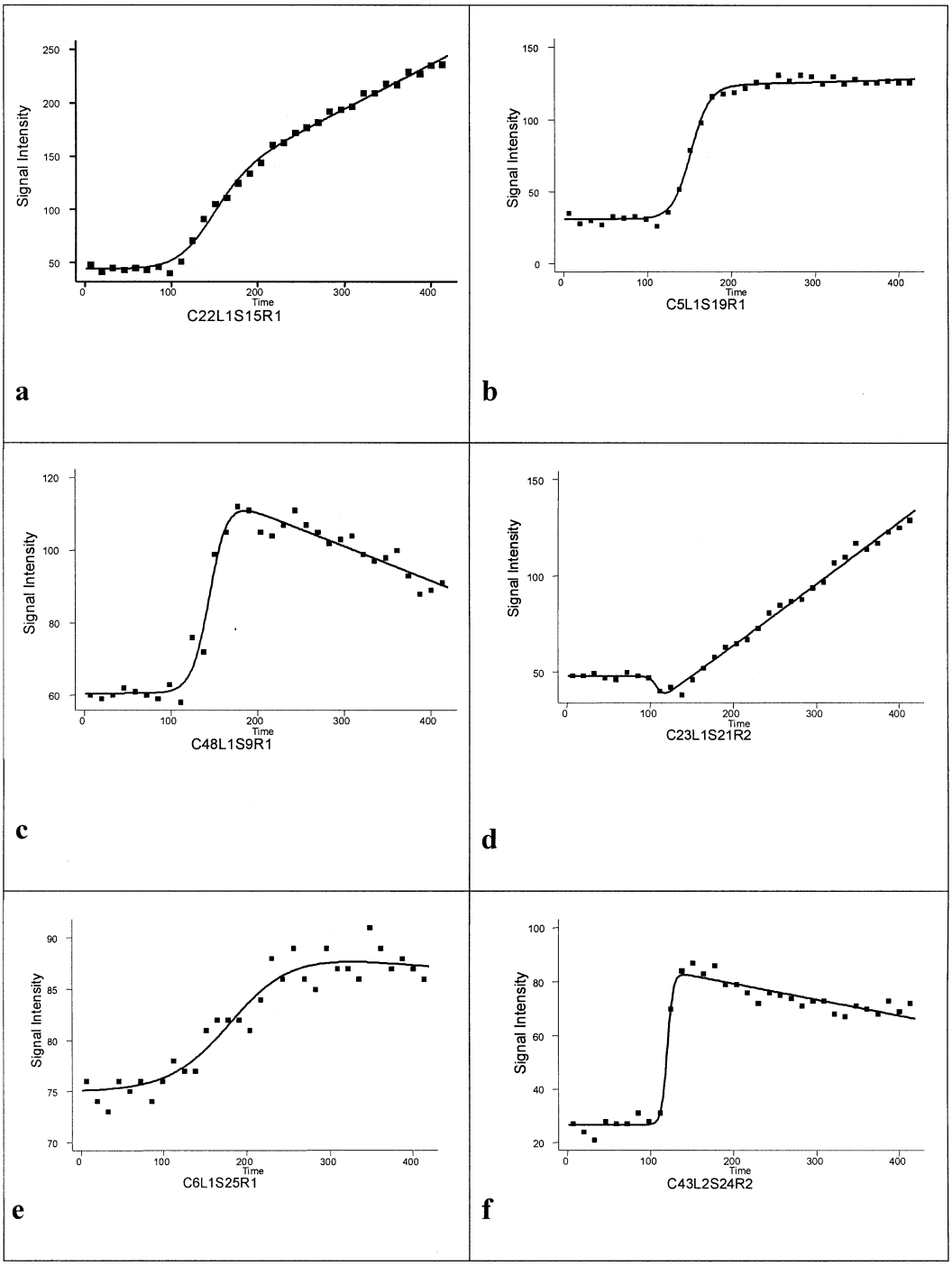

Fig. 2. Signal intensity versus time (secs) curves from six breast tumors: (a) benign fibroadenoma with proliferative fibrocystic changes without atypia; (b) infiltrating and in situ ductal carcinoma; (c) infiltrating ductal carcinoma; (d) adenocarcinoma; (e) benign fibroadenoma, (f) cancer. Note, in each case, the signal intensity axis has been rescaled to better display the goodness of fit of each curve.

rameter P_4, despite the fact that there was only one datum where the signal intensity curve was steeply rising.

The signal intensity curve shown in Fig. 2a was from a benign tumor identified as a fibroadenoma with proliferative fibrocystic changes without atypia. The P_2 and P_4 parameters for this curve were relatively small, while P_5 was substantial and positive (Table 1). The curve shown in Fig. 2e was also from a benign tumor (fibroadenoma). Parameters of the curves shown in Fig. 2a and 2e typify those for benign tumors. The curve shown in Fig. 2b was from an infiltrating and in situ ductal carcinoma and the curves shown in Fig. 2c and 2f were also from cancerous tumors. In contrast to the benign tumor parameters, the P_2 and P_4 for the cancerous tumors shown in Fig. 2b, 2c and 2f are

Table 1
Model parameters, their standard deviations, Model R^2 and RMSE as well as secondary parameters for the cases shown in Fig. 2

Case	a	b	c	d	e	f
Pathology	Benign	Cancer	Cancer	Cancer	Benign	Cancer
Primary parameters						
P_1	44 ± 2.6	31 ± 2.7	61 ± 1.4	48 ± 1.3	75 ± 1.2	27 ± 3.0
P_2	27 ± 6.9	90 ± 3.6	69 ± 3.6	−48 ± 1.8	15 ± 5.2	65 ± 2.3
P_3 (sec)	141 ± 3.3	152 ± 1.2	145 ± 2.1	109 ± 3.7	183 ± 18.2	121 ± 1.2
P_4*10^{-2} (sec^{-1})	4.8 ± 0.56	9.0 ± 0.80	9.7 ± 1.58	24.5 ± 18.9	2.7 ± 0.62	28.1 ± 6.16
P_5*10^{-2} (sec^{-1})	41 ± 2.1	2 ± 1.2	−9 ± 1.2	32 ± 0.6	−1 ± 1.4	−6 ± 0.8
R_a^2	0.9991	0.9991	0.9988	0.9991	0.9997	0.9981
RMSE	4.63	3.18	3.39	2.58	1.57	3.05
Secondary parameters						
MS (sec^{-1})	0.3 ± 0.06	2.0 ± 0.16	1.7 ± 0.23	−2.7 ± 13.05	0.1 ± 0.02	4.5 ± 0.70
SEMS	43 ± 2.5	47 ± 1.0	28 ± 1.0	−7 ± 4.0	7 ± 1.4	28 ± 0.5
PSR	84 ± 1.9	74 ± 1.5	42 ± 0.8	−9 ± 2.0	11 ± 0.6	44 ± 2.0
BSP (sec)	120 ± 2.0	137 ± 1.7	131 ± 2.9	102 ± 1.1	137 ± 5.7	116 ± 6.2
ESP (sec)	176 ± 3.5	167 ± 1.2	158 ± 2.0	114 ± 12.0	228 ± 13.9	125 ± 6.3
WOR (sec)	56 ± 4.0	30 ± 2.1	27 ± 3.5	12 ± 12.1	90 ± 15.0	9 ± 8.8
AUC_{BE} (sec)	2931 ± 272	1414 ± 98	722 ± 91	−67 ± NC	650 ± 114	256 ± 44
$AUC_{420}*10^4$ (sec)	4.0 ± 0.17	2.6 ± 0.03	1.2 ± 0.03	1.1 ± 0.03	0.3 ± 0.03	1.5 ± 0.02

NC = not calculable

relatively substantial and positive, while the P_5 parameter is either close to zero or substantially negative. The unusual shape of the curve shown in Fig. 2d is due to the substantial negative value (−48) for parameter P_2. Because we have not encountered many curves of this shape we are unable to say if this shape of curve has diagnostic value, nor can we, at this stage, suggest a physiological explanation for this type of curve.

3.1. Secondary parameters

Some researchers have advocated using a variety of secondary diagnostic parameters derivable from the signal intensity curve. These include: presence or absence of enhancement, maximum slope (*MS*), maximum amplitude, enhancement at 1 min, etc. [24]. These are all derivable from the modified logistic function. Indeed, the modified logistic equation approach enables the secondary parameters shown in Table 1, to be derived in a more mathematically rigorous and accurate manner than similar heuristic parameters that others have derived manually [2,15–17]. For example, in Table 1, the *MS* parameter was well identified for all tumors except for the tumor with the atypical signal response curve shown in Fig. 2d. The same can be said for the signal enhancement at the maximum slope (*SEMS*). The remaining secondary parameters shown in Table 1 are generally well identified for all of the tumors shown. It can be seen in Fig. 1b that the *BSP* parameter is related to the time at which the period of linear uptake of contrast agent in the tumor begins. In our case, the absolute magnitude of *BSP* is somewhat arbitrary since it includes the time (98 s) for eight pre-injection signal-capturing events. *BSP* may also be susceptible to delays associated with inadvertently long injection protocol, asynchrony in timing the injection and re-starting the MRI capturing sequence, variation in the timing and duration of the saline flush and phenomena unassociated with the tumor, such as individual patient blood-flow dynamics. Nevertheless, as would be expected and as can be seen in Table 1, *BSP* is inversely correlated with P_4. In contrast to *BSP, WOR* should not be influenced by asynchrony in timing the injection with re-starting the MRI capturing sequence or pre-tumor blood dynamics and should therefore be more closely influenced by the uptake of contrast agent by the tumor. Indeed, from Table 1 it is clear that *WOR* is inversely related to the magnitude of P_4. From Table 1, cases "a" and "e", which were benign tumors, had the greatest and smallest AUC_{420}, respectively; so this parameter does not appear useful for diagnostic purposes. Similarly, AUC_{BE} does not offer diagnostic potential. Thus, although secondary parameters may correspond to some specific attributes of the signal intensity curve, the primary parameters are more appropriate for diagnostic purposes because they contain, in a succinct form, all of the information embedded in the signal intensity curves.

3.2. Standardization

In this exploration of MRI signal intensity curves, we have modeled the raw signal obtained from the MRI scanner. In contrast, some researchers first transform the signal before they attempt to extract signal attributes. For example, some researchers transform the signal in this fashion [9,25]:

$$SI*(t) = \frac{SI(t)}{P_1} \tag{6}$$

where $SI*(t)$ is the transformed signal. Other researchers transform the signal slightly differently [5,26]:

$$SI*(t) = \frac{SI(t) - P_1}{P_1} \quad (7)$$

If the system describing Gadolinium kinetics is linear, then such transformations should have little effect on the shape of the signal response curve. Indeed, if the transformation shown in Eq. (6) is carried out, then *SI*(t)* can be expressed as follows:

$$SI*(t) = \frac{P_2^* + (P_5^* \cdot t)}{\{1 + exp(-P_4 \cdot (t - P_3))\}} + P_1^* \quad (8)$$

where P_1^* equals 1, P_2^* equals $\frac{P_2}{P_1}$, P_5^* equals $\frac{P_5}{P_1}$ and P_3 and P_4 are as defined for Eq. (3).

If the transformation shown in Eq. (7) is employed, Eq. (8) also applies, but in this case P_1^* equals 0. Thus, in either case, the modified logistic equation can still be used to describe *SI*(t)*. In contrast to the above standardization procedures, Port et al. [12] used a complex compartmental model in which "tumor scale parameters were standardized by dividing them by the ratio of individual aorta scale parameter, G_A, over the mean population aorta scale parameter in order to eliminate the effect of inter-individual variability in V_1". In the Port et al. model, V_1 represents a central compartment (blood plasma). Such a transformation as advocated by Port et al. is likely to lead to loss of information. Nevertheless, no matter the manner in which individual researchers transform the MRI signal, the modified logistic model presented here has the flexibility to fit such curves.

Some researchers inject the CR over a short time (10 to 30 s) [27] and others infuse the CR over longer periods ranging from 1 to 4 min [9, 12]. Thus, the duration of the injection or infusion may coincide with a substantial part of the period when the CR is being taken up by the tumor. The parameter describing the uptake of CR can therefore be greatly influenced by the infusion protocol. In the compartmental approach advocated by many researchers [5,9], the MRI signal or a transformed version of it, is modeled after t_0 where t_0 is the time of the injection. With respect to the compartmental model approach, one immediately obvious difficulty is the choice of what constitutes time zero. The researcher must decide if it is the beginning, middle or end of the injection/infusion period. This somewhat arbitrary decision will clearly impact greatly on the magnitude of estimated uptake rates as calculated by the compartmental approach. In contrast, by using the heuristic approach/modified logistic equation, it can be shown that the time of the injection has little impact on P_4 (the primary parameter describing the uptake of CR), but that the potentially confounding effect of time of injection as well as delay and dispersion effects are accommodated by the nuisance parameter P_3 [13]. However, the importance of P_3 to the global fitting of the heuristic model to data should not be ignored. For example, comparative sensitivity analysis of

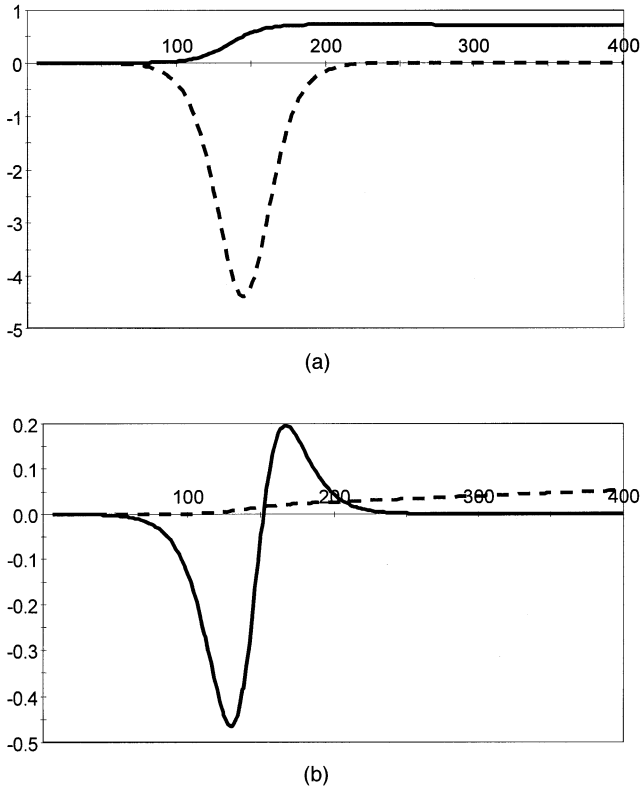

Fig. 3. (a) Relative sensitivities of *SI(t)* versus time (secs) with respect to parameters P_2 (solid line) and P_3 (dashed line). (b) Relative sensitivities of *SI(t)* with respect to parameters P_4 (solid line) and P_5 (dashed line).

SI(t) with respect to parameters P_2, P_3, P_4 and P_5 for tumor 'b' (see Fig. 3a and 3b) demonstrates that in a relative sense, *SI(t)* is most sensitive to changes in P_3 when *SI(t)* is most rapidly increasing, and that in order to accurately estimate P_3, and fit the model to the data, frequent sampling is indicated in this time domain.

4. Conclusion

In conclusion, the heuristic model presented here has the flexibility to accurately describe all of the MR signal enhancement patterns that we have encountered. The heuristic model has five primary parameters, but three of these: P_2, P_4 and P_5 appear to describe the principal attributes of the signal enhancement curve that other researches have shown to have diagnostic/prognostic value. The parameters of the heuristic model can be used to accurately estimate a number of secondary parameters that have previously also been shown to have diagnostic value.

Acknowledgments

This work was supported by grants from the NIH (CA82707-01, CA090699-0182) and by a grant from the

Susan G. Komen Breast Cancer Foundation (IMG 2000-224).

References

[1] Cannard L, Lemelle JL, Gaconnet E, Champigneulle J, Mainard L, Claudon M. Dynamic MR imaging of bladder haemangioma. Pediat Radiol 2001;31:882–5.
[2] Fujii K, Fujita N, Hirabuki N, Hashimoto T, Miura T, Kozuka T. Neuromas and meningiomas: evaluation of early enhancement with dynamic MR imaging. AJNR Am J Neuroradiol 1992;13:1215–20.
[3] Furman-Haran E, Grobgeld D, Degani H. Dynamic contrast-enhanced imaging and analysis at high spatial resolution of MCF7 human breast tumors. J Magn Reson 1997;128:161–71.
[4] Parker GJ, Tofts PS. Pharmacokinetic analysis of neoplasms using contrast-enhanced dynamic magnetic resonance imaging. Top Magn Reson Imaging 1999;10:130–42.
[5] Tofts PS, Berkowitz B, Schnall MD. Quantitative analysis of dynamic Gd-DTPA enhancement in breast tumors using a permeability model. Magn Reson Med 1995;33:564–8.
[6] Hulka CA, Edmister WB, Smith BL, et al. Dynamic echo-planar imaging of the breast: experience in diagnosing breast carcinoma and correlation with tumor angiogenesis. Radiology 1997;205:837–42.
[7] Tofts PS. Modeling tracer kinetics in dynamic Gd-DTPA MR imaging. J Magn Reson Imaging 1997;7:91–101.
[8] Tofts PS, Brix G, Buckley DL, et al. Estimating kinetic parameters from dynamic contrast-enhanced T(1)-weighted MRI of a diffusable tracer: standardized quantities and symbols. J Magn Reson Imaging 1999;10:223–32.
[9] Brix G, Semmler W, Port R, Schad LR, Layer G, Lorenz WJ. Pharmacokinetic parameters in CNS Gd-DTPA enhanced MR imaging. J Comput Assist Tomogr 1991;15:621–8.
[10] Larsson HB, Stubgaard M, Frederiksen JL, Jensen M, Henriksen O, Paulson OB. Quantitation of blood-brain barrier defect by magnetic resonance imaging and gadolinium-DTPA in patients with multiple sclerosis and brain tumors. Magn Reson Med 1990;16:117–31.
[11] Berman M, Schoenfeld R. Invariants in experimental data on linear kinetics and the formulation of models. J Appl Phys 1956;27:1361–70.
[12] Port RE, Knopp MV, Hoffmann U, Milker-Zabel S, Brix G. Multicompartment analysis of gadolinium chelate kinetics: blood-tissue exchange in mammary tumors as monitored by dynamic MR imaging. J Magn Reson Imaging 1999;10:233–41.
[13] Calamante F, Gadian DG, Connelly A. Delay and dispersion effects in dynamic susceptibility contrast MRI: simulations using singular value decomposition. Magn Reson Med 2000;44:466–73.
[14] Mussurakis S, Buckley DL, Bowsley SJ, et al. Dynamic contrast-enhanced magnetic resonance imaging of the breast combined with pharmacokinetic analysis of gadolinium-DTPA uptake in the diagnosis of local recurrence of early stage breast carcinoma. Invest Radiol 1995;30:650–62.
[15] Brown J, Buckley D, Coulthard A, et al. Magnetic resonance imaging screening in women at genetic risk of breast cancer: imaging and analysis protocol for the UK multicentre study. UK MRI Breast Screening Study Advisory Group. Magn Reson Imaging 2000;18:765–76.
[16] Kaiser WA, Zeitler E. MR imaging of the breast: fast imaging sequences with and without Gd-DTPA. Preliminary observations. Radiology 1989;170:681–6.
[17] Kuhl CK, Mielcareck P, Klaschik S, et al. Dynamic breast MR imaging: are signal intensity time course data useful for differential diagnosis of enhancing lesions [comment]? Radiology 1999;211:101–10.
[18] Mayr NA, Yuh WT, Magnotta VA, et al. Tumor perfusion studies using fast magnetic resonance imaging technique in advanced cervical cancer: a new noninvasive predictive assay [comment]. Int J Radiat Oncol Biol Phys 1996;36:623–33.
[19] Suga K, Ogasawara N, Yuan Y, Okada M, Matsunaga N, Tangoku A. Visualization of breast lymphatic pathways with an indirect computed tomography lymphography using a nonionic monometric contrast medium iopamidol: preliminary results. Invest Radiol 2003;38:73–84.
[20] Song HK, Dougherty L, Schnall MD. Simultaneous acquisition of multiple resolution images for dynamic contrast enhanced imaging of the breast. Magn Reson Med 2001;46:503–9.
[21] Stata. Stata Statistical Software. In Release 7.0 ed. College Station, TX: Stata Corporation; 2001.
[22] Stefanovski D, Moate PJ, Boston RC. WinSAAM: a windows-based compartmental modeling system. Metabolism 2003;52:1153–66.
[23] Wastney ME, Patterson BH, Linares OA, Greif PC, Boston RC. Investigating biological systems using modeling—strategies and software. 1st ed. San Diego: Academic Press, 1999.
[24] Padhani AR, Husband JE. Dynamic contrast-enhanced MRI studies in oncology with an emphasis on quantification, validation and human studies. Clin Radiol 2001;56:607–20.
[25] Landis CS, Li X, Telang FW, et al. Determination of the MRI contrast agent concentration time course in vivo following bolus injection: effect of equilibrium transcytolemmal water exchange. Magn Reson Med 2000;44:563–74.
[26] Buckley DL, Kerslake RW, Blackband SJ, Horsman A. Quantitative analysis of multi-slice Gd-DTPA enhanced dynamic MR images using an automated simplex minimization procedure. Magn Reson Med 1994;32:646–51.
[27] Tofts PS, Berkowitz BA. Measurement of capillary permeability from the Gd enhancement curve: a comparison of bolus and constant infusion injection methods. Magn Reson Imaging 1994;12:81–91.